Quantum Phases from Competing Van der Waals and Dipole-Dipole Interactions of Rydberg Atoms

Zeki Zeybek,[1,2,*] Rick Mukherjee,[2,†] and Peter Schmelcher[1,2]
[1]The Hamburg Centre for Ultrafast Imaging, Universität Hamburg Luruper Chaussee 149, 22761 Hamburg, Germany
[2]Zentrum für Optische Quantentechnologien, Universität Hamburg Luruper Chaussee 149, 22761 Hamburg, Germany

(Received 30 March 2023; accepted 2 October 2023; published 15 November 2023)

Competing short- and long-range interactions represent distinguished ingredients for the formation of complex quantum many-body phases. Their study is hard to realize with conventional quantum simulators. In this regard, Rydberg atoms provide an exception as their excited manifold of states have both density-density and exchange interactions whose strength and range can vary considerably. Focusing on one-dimensional systems, we leverage the Van der Waals and dipole-dipole interactions of the Rydberg atoms to obtain the zero-temperature phase diagram for a uniform chain and a dimer model. For the uniform chain, we can influence the boundaries between ordered phases and a Luttinger liquid phase. For the dimerized case, a new type of bond-order-density-wave phase is identified. This demonstrates the versatility of the Rydberg platform in studying physics involving short- and long-ranged interactions simultaneously.

DOI: 10.1103/PhysRevLett.131.203003

Introduction.—The interplay of short- and long-range interactions gives rise to diverse phenomena with implications in different areas such as study of electronic dynamics and stability in proteins [1–4], self-assembly in polymers [5], and exotic quantum phases in condensed matter physics [6–10]. However, the study of these phenomena in the natural biochemical and solid-state setups are challenging due to the limited control and the finite temperature environments. This has led to a rapid growth in the use of ultracold systems for quantum simulation of many-body problems [11–13]. These include the highly tunable short-range interactions with atoms in optical lattices [14,15] to long-range interacting dipolar gases [16,17], polar molecules [18–21], and trapped ions [22–24]. Realizing interactions with different scaling is of great interest not only to the broader condensed matter community, but also from a different viewpoint, it opens avenues for simulating chemical and biological processes that involve short- and long-range physics [1–5]. This is particularly challenging since it requires implementing different power-law interactions simultaneously, where other quantum simulating platforms such as trapped ions have limited utility.

Platforms based on neutral Rydberg atoms have proven to be highly practical quantum simulators [25–29] as their large dipole moments provide tunable strong interactions that range from dipole-dipole ($1/r^3$ scaling) to Van der Waals ($1/r^6$ scaling). Rydberg dressing [30,31] allows for a certain flexibility in controlling short- and long-range interactions simultaneously with applications in many-body physics [32,33], but they can be experimentally challenging to realize [34,35]. Currently, the most common approach adopted in the context of quantum simulation with Rydberg atoms is to focus either on short-range (VdW) [36–43] or long-range (dipolar) interactions [44–47], but rarely both [48]. In the past, theoretical studies [49,50] were motivated by the limitations of the experiments to focus on either regime but never both. Only recently, experiments were performed with a pair of Rydberg states that potentially allow both ranges of interactions [44,51] but were never comprehensively exploited.

In this Letter, we propose an alternative approach to study short- and long-range physics by combining the effects of Van der Waals and dipole-dipole interactions of Rydberg atoms. Using the one-dimensional (1D) uniform and dimerized lattices, we study the ground state phase diagram and unveil the flexibility in accessing different regimes of the ordered and liquid phases. For the uniform chain, the competition between the interactions is reflected in the competing boundaries between the gapless Luttinger liquid (LL) and the gapped density-wave (DW) ordered phases. In the dimerized chain, apart from realizing the individual phases of bond-order (BO) and DW, we find unique bond-order-density-wave (BODW) phase that has not been previously explored using conventional dimerized model [52,53].

Model and Hamiltonian.—We discuss the Rydberg setup and its mapping to extended Bose-Hubbard model that distinguishes itself from existing bosonic models [42,43,54,55]. The uniform and dimerized lattices are considered where the latter is known for rich physics involving topological and insulating phases [53,56–60].

As illustrated in Fig. 1, the setup consists of a linear chain of trapped atoms that could either have uniform or dimerized lattice configurations. Each atom is a two-level

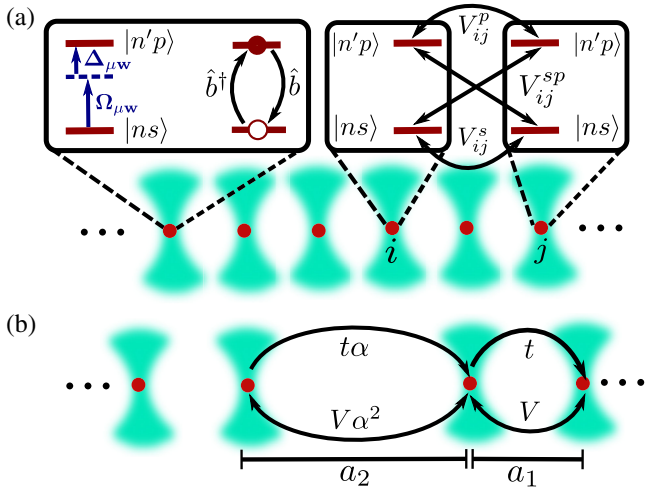

FIG. 1. (a) Diagram depicting a uniform lattice of neutral atoms treated as two-level systems consisting of highly excited Rydberg states. Microwave laser with Rabi frequency $\Omega_{\mu w}$ and detuning $\Delta_{\mu w}$ couples the levels. Atoms in the same Rydberg state experience VdW interactions with strengths V_{ij}^s, V_{ij}^p, while V_{ij}^{sp} tunes the dipolar exchange interaction between different levels. The two-level system encodes the presence (absence) of a boson at a given site defined by $\hat{b}^\dagger(\hat{b})$. (b) Dimerized chain with alternating intracell a_1 and intercell a_2 lattice constants with corresponding hopping $(t, t\alpha)$ and off-site interactions $(V, V\alpha^2)$.

system made of $|ns\rangle$ and $|n'p\rangle$ Rydberg states, where n, n' are principal quantum numbers. Unlike most Rydberg simulators with one ground state and a Rydberg level, the pair of Rydberg states considered here allows the system to have two types of interactions that differ in range and character: (i) the short-range Van der Waals (VdW) interactions between the $ns-ns$ and $n'p-n'p$ and (ii) the long-range dipolar interaction that causes a state exchange between atoms in different Rydberg levels $ns-n'p$. The Rydberg interactions along with the microwave laser coupling between $|ns\rangle$ and $|n'p\rangle$ levels are all schematically shown in Fig. 1(a). The corresponding atomic Hamiltonian describing the full setup with uniform lattice spacing a is given as

$$\hat{H}_A = \sum_i \left[\frac{\Omega_{\mu w}}{2}(\hat{\sigma}_i^{sp} + \hat{\sigma}_i^{ps}) - \Delta_{\mu w}\hat{\sigma}_i^{pp}\right] + V^p \sum_{i<j} \frac{\hat{\sigma}_i^{pp}\hat{\sigma}_j^{pp}}{|i-j|^6} + V^s \sum_{i<j} \frac{\hat{\sigma}_i^{ss}\hat{\sigma}_j^{ss}}{|i-j|^6} + V^{sp} \sum_{i<j} \left(\frac{\hat{\sigma}_i^{sp}\hat{\sigma}_j^{ps}}{|i-j|^3} + \text{H.c.}\right). \quad (1)$$

Here, $\hat{\sigma}_i^{\alpha\beta} = |\alpha\rangle_i\langle\beta|$ is the projection operator to the relevant atomic state with $\alpha, \beta \in \{|ns\rangle, |n'p\rangle\}$ at site i. $V^p = C_6^p/a^6$ and $V^s = C_6^s/a^6$ are the strength of VdW interactions, where C_6^s and C_6^p are the dispersion coefficients. $V^{sp} = C_3/a^3$ is the dipole-dipole interaction strength with C_3 as the exchange coefficient. There are experimental realizations of the above Hamiltonian [44,51].

In order to represent Eq. (1) in the Bose-Hubbard picture, the occupation of state $|n'p\rangle$ at site i is associated with the presence of a boson at that site and denoted by $|\bullet\rangle_i$ while $|\circ\rangle_i$ means the absence of a boson that implies the occupation of state $|ns\rangle$. With these definitions, an arbitrary state $|ns\, n'p\, n'p\, ns\ldots\rangle$ is written as $|\circ\bullet\bullet\circ\ldots\rangle$. Since each atom cannot have more than one excitation $|n'p\rangle$, having two particles at the same site is prohibited, which imposes a hard-core constraint. Defining the $\hat{b}^\dagger(\hat{b})$ as the bosonic creation (annihilation) operator, $\hat{H}_A$ is rewritten as follows:

$$\hat{H}_{e\text{BH}} = \sum_{i<j} t_{ij}(\hat{b}_i^\dagger \hat{b}_j + \text{H.c.}) + \sum_{i<j} V_{ij}\hat{n}_i\hat{n}_j - \sum_i (\Delta_{\mu w} + \mathcal{I}_i)\hat{n}_i + \frac{\Omega_{\mu w}}{2}\sum_i (\hat{b}_i^\dagger + \hat{b}_i), \quad (2)$$

where we used the mapping $\hat{\sigma}^{ps} \to \hat{b}^\dagger$, $\hat{\sigma}^{pp} \to \hat{n} = \hat{b}^\dagger\hat{b}$, and $\hat{\sigma}^{ss} \to \mathbb{1} - \hat{n}$ with $(\hat{b}_i^\dagger)^2 = 0$. The first term in Eq. (2) is the long-range hopping $t_{ij} = V^{sp}/|i-j|^3$ that is encoded by the dipolar exchange interaction. $V_{ij} = V/|i-j|^6$ is the repulsive off-site density interaction, where $V = V^s + V^p = C_6/a^6$ and $C_6 = C_6^s + C_6^p$ is the combined dispersion coefficient. The chemical potential $(\Delta_{\mu w} + \mathcal{I}_i)$ determines the density of excitations $|n'p\rangle$ (number of bosons) in a lattice. The site-dependent contribution $\mathcal{I}_i = \sum_{i\neq j}(V^s/|i-j|^6)$ is an energy offset for a fixed value of the chemical potential and can be ignored in the bulk, thus $\mu_i \to \mu = \Delta_{\mu w}$. The $\hat{H}_{e\text{BH}}$ differs from other extended Bose-Hubbard models [42,43,54,55] in several aspects: (*i*) the existence of longer-range hopping and interactions and (*ii*) the last term in $\hat{H}_{e\text{BH}}$ breaks the global U(1) symmetry causing the number of bosons to be a non-conserved quantity. These aspects will play a role in the phase diagrams obtained later.

Figure 1(b) depicts the dimerized configuration formed by two sublattices with alternating lattice constants a_1 and a_2. The dimerized version of Eq. (2) is provided in [61], whose many-body energy spectrum for $\Omega_{\mu w} = 0$ comprises many distinct manifolds, each of which is characterized by a fixed number of bosons. For large negative values of the microwave detuning $\Delta_{\mu w}$, one obtains a completely empty lattice (all atoms in $|ns\rangle$ state). As $\Delta_{\mu w}$ increases, the number of bosons added to the lattice also increases. Similar to experiment [44], an adiabatic sweep through the parameters $[\Omega_{\mu w}(t), \Delta_{\mu w}(t)]$ can take the lattice system of size L from one manifold with zero bosons to another manifold of N bosons giving a filling $\rho = N/L$. After reaching a given filling ρ, the microwave laser is switched off and the following Hamiltonian is written as

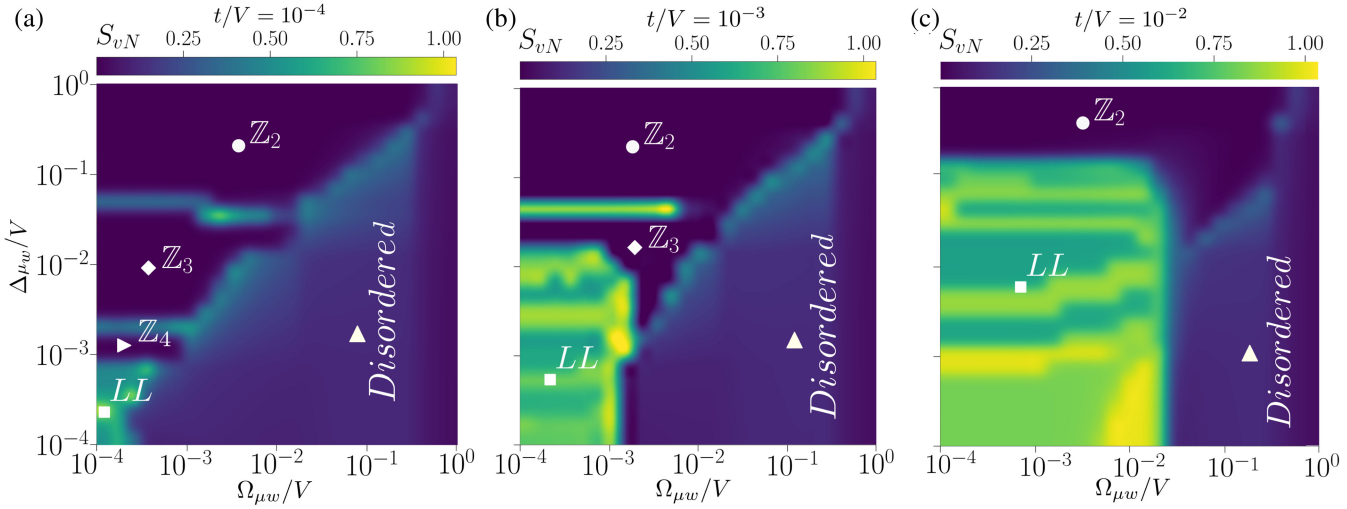

FIG. 2. Phase diagrams showing the ground state entanglement entropy S_{vN} of $\hat{H}_{e\mathrm{BH}}$ in the $(\Delta_{\mu w}, \Omega_{\mu w})$ parameter space for system size $L = 121$ with varying t/V in (a)–(c), respectively. The dark-shaded blue lobes in the top left part of the phase diagrams represent vanishing S_{vN} that correspond to different gapped ordered phases $Z_{q=2,3,4}$. The yellow-green regions represent finite S_{vN} corresponding to the gapless Luttinger liquid (LL) phase. For large values of $\Omega_{\mu w}$, one obtains the disordered phase, which is shown as light-shaded blue. Verification of the individual phases is provided in [61].

$$\hat{H}_{\mathrm{dim}} = t \sum_{i\in\mathrm{odd}} (\hat{b}_i^\dagger \hat{b}_{i+1} + \mathrm{H.c.}) + t\alpha \sum_{i\in\mathrm{even}} (\hat{b}_i^\dagger \hat{b}_{i+1} + \mathrm{H.c.}) + V \sum_{i\in\mathrm{odd}} \hat{n}_i \hat{n}_{i+1} + V\alpha^2 \sum_{i\in\mathrm{even}} \hat{n}_i \hat{n}_{i+1} + \hat{H}_{\mathrm{LR}}. \quad (3)$$

The even and odd sums represent the intra- and intercell terms, respectively, and the dimerization constant $\alpha = (a_1/a_2)^3$ controls the degree of dimerization in the lattice. $t = -C_3/a_1^3$ and $V = C_6/a_1^6$ are the intracell hopping and off-site interaction strengths, respectively, with $C_6, C_3 > 0$. $\hat{H}_{\mathrm{dim}}$ deviates from existing dimer models [53,58–60] in the sense that it has both local as well as long-range hopping and off-site interaction defined under $\hat{H}_{\mathrm{LR}}$ (explicitly given in [61]). The fact that it has dimerization in interaction and not just in hopping will play a crucial role in the phase diagrams.

Results.—Figures 2 and 3 are the ground state phase diagrams for $\hat{H}_{e\mathrm{BH}}$ and $\hat{H}_{\mathrm{dim}}$ obtained using finite-size density matrix renormalization group (DMRG) [70,71]. More details about numerics are in [61]. In earlier works for a uniform lattice [36,49,50,72], one finds the LL phase to be always dominated by the ordered phases for the entire region of allowed laser parameters. In contrast, here we show that the boundaries between ordered and LL phases are easily adjustable, and find scenarios where LL even dominates. This is possible due to the competition of VdW and dipolar exchange terms. The same flexibility in the boundaries of the BODW phases are seen in the dimerized case. Moreover, the existence of BODW phase for $\rho = 1/3$ filling is shown, which does not occur in conventional models [52,53].

In Figs. 2(a)–2(c), we compute the half-chain bipartite entanglement entropy $S_{vN} \equiv -\mathrm{Tr}(\rho_r \ln \rho_r)$ of the ground state over the parameter space $(\Omega_{\mu w}, \Delta_{\mu w})$ for fixed hopping t, where ρ_r is the reduced density matrix of half of the chain. This has been performed for a varying relative strength of the hopping t as shown in Figs. 2(a)–2(c). DWs are many-body ground states that are ordered (crystalline) and are characterized with unit cell p/q where p denotes the number of bosons and q is the size of the unit cell. For example, the circle markers in Figs. 2(a)–(c) correspond to phases that break $\mathbb{Z}_2$ translational symmetry with $p/q = 1/2$. $\mathbb{Z}_2$ phase is described by the state $|\bullet\circ\bullet\ldots\bullet\circ\bullet\rangle$, which is a product state and thus possesses a vanishing S_{vN}. Similarly, higher period DW phases ($\mathbb{Z}_{q=3,4}$) are also shown in Figs. 2(a) and 2(b).

Although both the hopping term t and Rabi coupling $\Omega_{\mu w}$ introduce quantum fluctuations to the system, they have different effects on the ordered states. For example, if $\Omega_{\mu w} \gg t$, then one obtains a disordered state. However, when $\Omega_{\mu w}$ becomes comparable to t, then we have either an ordered phase or a LL phase depending on the value of $\Delta_{\mu w}$. Close to the classical regime ($\Omega_{\mu w} = t \simeq 0$), the range of the ordered phase $\mathbb{Z}_q$ in terms of the detuning is given as $\delta\Delta_{\mu w} \sim V_{i,i+q-1} + \mathcal{O}(V_{i,i+q})$ [50,73]. Thus, for low values of $(t, \Omega_{\mu w})$, one finds a host of ordered phases $\mathbb{Z}_{q=2,3,4}$ as seen in Fig. 2(a). As t increases such that $t \geq V_{i,i+q-1}$, then ordered phases with unit cells larger than q get washed out and instead the LL phase takes over as seen in Figs. 2(b) and 2(c). This condition is satisfied as the VdW interaction has the combined effect of ns and $n'p$ states for different n and n' [61]. Universal properties of the LL phase such as

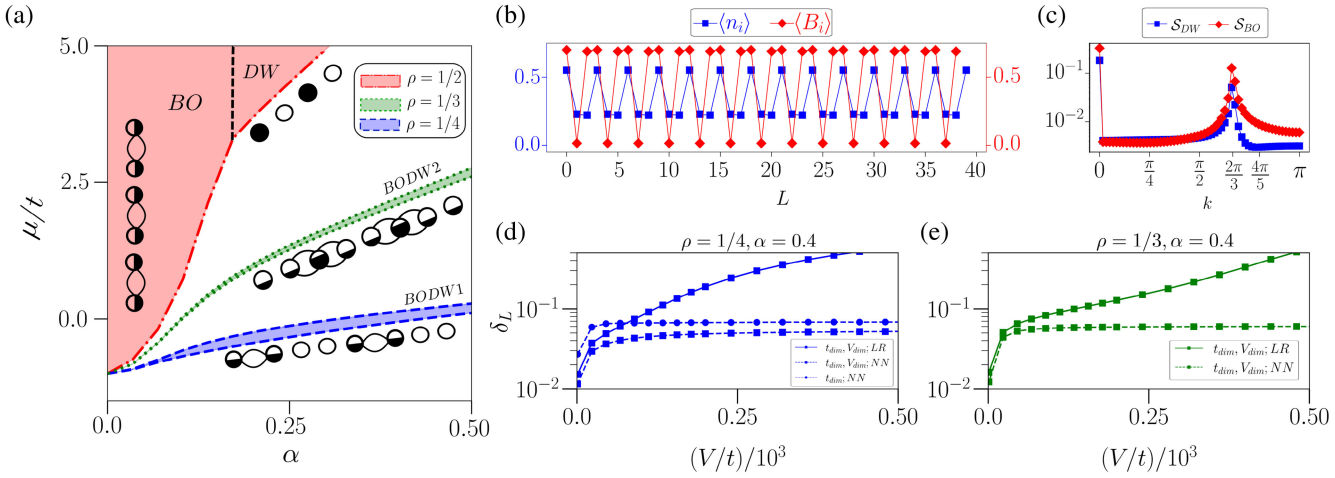

FIG. 3. (a) Gapped phases of $\hat{H}_{\text{dim}}$ are shown as a function of α with fixed $V/t = 200$ for system size $L = 240$. The red dashed-dotted line defines the lower boundary at $\rho = 1/2$ with the vertical dashed black line that separates the BO and DW regions. The green dotted and the blue dashed lines determine the boundaries of the BODW phases at $\rho = 1/3$ and $\rho = 1/4$, respectively. Density and bond formation in each phase are symbolically represented with partially filled circles (superposition of ns and $n'p$ states) and curved lines between sites, respectively. (b) Expectation values of the bond energy (red, diamond) and density (blue, square) operators for the BODW phase at $\rho = 1/3$ for $\alpha = 0.4$ and $V/t = 200$ is displayed. The corresponding structure factors are shown in (c). (d),(e) Figure comparing the gap δ_L for BODW phases at filling $\rho = 1/4$ and $\rho = 1/3$ is shown with different types of couplings in Eq. (3). The gap δ_L is plotted as a function of V/t with fixed α and system size $L = 240$. Cases with (squares) and without (circles) dimerization in the interaction are considered for different range of interactions: nearest neighbor (dashed line with NN) and long range (solid line with LR).

power-law decay of correlations and the central charge $c = 1$ [74,75] have been verified [61].

Figure 3(a) is obtained by determining the single-particle excitation gap $\delta_L(\alpha, V) = \mu^+(\alpha, V) - \mu^-(\alpha, V)$ as a function of α with fixed V. Thus, the extent of the gapped phases in the phase diagram scales as δ_L. Here, $\mu^+ = E(N+1) - E(N)$ and $\mu^- = E(N) - E(N-1)$ are the chemical potentials that define the boundaries of the gapped phases for a given filling ρ and $E(N)$ is the ground state energy for a system of N bosons defined by $\hat{H}_{\text{dim}}$. In Fig. 3(a), four types of gapped phases (DW, BO, BODW1, BODW2) are obtained for different values of filling ρ in the (α, μ) parameter space with constant V. DWs are the ordered phases as discussed before while the BO phase is a product of independent dimers that is represented as $\prod_{i=0} (\frac{\hat{b}^\dagger_{2i} + \hat{b}^\dagger_{2i+1}}{\sqrt{2}}) |\circ\circ\cdots\circ\rangle = |\text{⚬⚬ ⚬⚬}\ldots\rangle$, where each dimer corresponds to two sites sharing a single delocalized boson (⚬⚬). Bond-order-density-wave (BODW) has the characteristic of both bond ordering and density wave ordering. Numerical verification of the individual phases is provided in [61].

In Fig. 3(a), at $\rho = 1/2$, the gap remains open for all values of α and hosts two different ordered phases, BO and DW. Low values of α is indicative of a highly dimerized lattice where the nearest-neighbor processes within a unit cell dominates over long-range processes such as intercell hopping and extended off-site interactions. At $\rho = 1/2$ filling, this means significant energy costs in adding or removing bosons that leads to a region of energy gap corresponding to the BO phase as seen in Fig. 3(a). As α is increased, the long-range effects of hopping and interaction become relevant. But if V/t is sufficiently large, which is the case in Fig. 3(a), then the repulsive VdW interaction leads to a DW phase for the $\rho = 1/2$ filling.

For any other filling $\rho \neq 1/2$, the gap closes as $\alpha \to 0$ as seen in Fig. 3(a), which implies that there is no energy cost in adding or removing bosons and allowing free movement of bosons across the lattice (LL phase) is favored over the BO phase as seen for $\rho = 1/4, 1/3$ fillings. As α increases, long-range processes become dominant and for sufficiently large V/t, BODW phases are obtained for $\rho = 1/4, 1/3$ fillings in contrast to the DW phase that we get for $\rho = 1/2$ filling. BODW phases arise from the cumulative effect of dominant long-range repulsive interactions at large values of α and the constraint of sharing certain number of bosons among the lattice due to the fixed filling fraction. However, it is sufficient to have nearest-neighbor interactions to stabilize the BODW1 phase [53], which consists of dimers in every alternating unit cell. Thus, the BODW1 phase can be described by a product state $\prod_{i=0} (\frac{\hat{b}^\dagger_{4i} + \hat{b}^\dagger_{4i+1}}{\sqrt{2}}) |\circ\circ\cdots\circ\rangle = |\text{⚬⚬ ○ ○ ⚬⚬ ○ ○}\ldots\rangle$ to a good approximation. Unlike BODW1, long-range interactions are needed to stabilize the BODW2 phase. Therefore, it cannot be described with independent dimers but rather is depicted as $|\text{⚬⚬⚬⚬⚬⚬}\ldots\rangle$, where a pair of dimers is shared between three sites. The latter BODW2 phase has not been explored before.

In Figs. 3(b) and 3(c), the characterization of the BODW phase at $\rho = 1/3$ is shown [61]. The BO nature

is probed with the bond order structure factor $\mathcal{S}_{\mathrm{BO}}(k) = (1/L^2)\sum_{i,j} e^{ikr}\langle \hat{B}_i \hat{B}_j \rangle$, where $\hat{B}_i = \hat{b}_i^\dagger \hat{b}_{i+1} +$ H.c. is the bond energy operator, while the density-wave structure factor is $\mathcal{S}_{\mathrm{DW}}(k) = (1/L^2)\sum_{i,j} e^{ikr}\langle \hat{n}_i \hat{n}_j \rangle$. In Fig. 3(b), oscillations in $\hat{n}_i$ imply that the bosons primarily occupy every third site on the chain (analogous to $\mathbb{Z}_{q=3}$), thus giving the DW character of the phase. BO oscillations point to a state with $p = 2$ bonds for a unit cell of size $q = 3$ as two bonds form among three sites. These findings are also reflected in the peaks of the structure factors $\mathcal{S}_{\mathrm{DW}}(k)$ and $\mathcal{S}_{\mathrm{BO}}(k)$ at $k = 2\pi/3$ as shown in Fig. 3(c). Figure 3(d) shows the gap δ_L for the BODW1 phase as a function V/t with fixed dimerization $\alpha = 0.4$ for different cases. One finds large energy gaps for the model with dimerized long-range interactions when compared to the almost vanishing gap for the nondimerized and nearest-neighbor dimerized interacting models. A similar analysis applies to BODW2 in Fig. 3(e). The key feature that is required to obtain the BODW2 phase is the necessity of beyond nearest-neighbor contributions along with dimerization in the interaction. However, the stability of the phases and thus their boundaries depend on the scaling of the interactions with distance. This highlights the key merits of our setup when compared to existing dimer models where only the hopping term is dimerized [53,57–60].

For the Rydberg states considered in this work, we have a lifetime of few hundreds of microseconds. This implies that for a chain of 10–20 atoms, the system lifetime is on the order of few tens of microseconds, which is sufficient for the phases to be experimentally realized while taking into account the relevant dissipative processes. A detailed analysis on the experimental feasibility is provided in [61].

Conclusion and outlook.—Many-body systems with interactions operating over different length scales host a wide range of phenomena in nature. This work promotes the quantum simulation of such phenomena using Rydberg atoms where the interplay between VdW and dipolar interactions provide a long-range dimerized Hubbard model. The ground state phase diagram of this model in 1D is characteristically distinct from conventional models in two key aspects: larger tunability for the LL phase in the uniform case and the existence of a novel BODW phase in the dimerized case. Future works will include the investigation of higher dimensional lattices, different geometries, and out-of-equilibrium dynamics with the recently developed multilayer multiconfigurational approach for spin systems [76].

This work is funded by the Cluster of Excellence "CUI: Advanced Imaging of Matter" of the Deutsche Forschungsgemeinschaft (DFG)—EXC 2056—Project ID 390715994. This work is funded by the German Federal Ministry of Education and Research within the funding program "quantum technologies—from basic research to market" under Contract No. 13N16138.

*zzeybek@physnet.uni-hamburg.de
†rmukherj@physnet.uni-hamburg.de

[1] S.-Y. Sheu, E. W. Schlag, and D.-Y. Yang, Phys. Chem. Chem. Phys. **17**, 23088 (2015).
[2] D. Gnandt and T. Koslowski, Phys. Chem. Chem. Phys. **21**, 18595 (2019).
[3] S. Miyazawa and R. L. Jernigan, Proteins **50**, 35 (2003).
[4] I. Alshareedah, T. Kaur, J. Ngo, H. Seppala, L.-A. D. Kounatse, W. Wang, M. M. Moosa, and P. R. Banerjee, J. Am. Chem. Soc. **141**, 14593 (2019).
[5] O. Patsahan, M. Litniewski, and A. Ciach, Soft Matter **17**, 2883 (2021).
[6] M. Baćani, M. Novak, F. Orbanić, K. Prša, I. Kokanović, and D. Babić, Phys. Rev. B **96**, 035104 (2017).
[7] F. Iglói, B. Blaß, G. m. H. Roósz, and H. Rieger, Phys. Rev. B **98**, 184415 (2018).
[8] M. Nishino, C. Enachescu, and S. Miyashita, Phys. Rev. B **100**, 134414 (2019).
[9] Y. Azouz, M. Benhamida, and K. Zanat, J. Magn. Magn. Mater. **559**, 169518 (2022).
[10] X. Zhu, Y. Huang, H. Guo, and S. Feng, Phys. Rev. B **106**, 075109 (2022).
[11] M. Lewenstein, A. Sanpera, V. Ahufinger, B. Damski, A. Sen(De), and U. Sen, Adv. Phys. **56**, 243 (2007).
[12] I. Bloch, J. Dalibard, and W. Zwerger, Rev. Mod. Phys. **80**, 885 (2008).
[13] I. Bloch, J. Dalibard, and S. Nascimbène, Nat. Phys. **8**, 267 (2012).
[14] R. Landig, L. Hruby, N. Dogra, M. Landini, R. Mottl, T. Donner, and T. Esslinger, Nature (London) **532**, 476 (2016).
[15] C. Gross and I. Bloch, Science **357**, 995 (2017).
[16] C. Trefzger, C. Menotti, B. Capogrosso-Sansone, and M. Lewenstein, J. Phys. B **44**, 193001 (2011).
[17] S. Baier, M. J. Mark, D. Petter, K. Aikawa, L. Chomaz, Z. Cai, M. Baranov, P. Zoller, and F. Ferlaino, Science **352**, 201 (2016).
[18] B. Yan, S. A. Moses, B. Gadway, J. P. Covey, K. R. A. Hazzard, A. M. Rey, D. S. Jin, and J. Ye, Nature (London) **501**, 521 (2013).
[19] K. R. A. Hazzard, B. Gadway, M. Foss-Feig, B. Yan, S. A. Moses, J. P. Covey, N. Y. Yao, M. D. Lukin, J. Ye, D. S. Jin, and A. M. Rey, Phys. Rev. Lett. **113**, 195302 (2014).
[20] A. Doçaj, M. L. Wall, R. Mukherjee, and K. R. A. Hazzard, Phys. Rev. Lett. **116**, 135301 (2016).
[21] M. Lemeshko, R. V. Krems, and H. Weimer, Phys. Rev. Lett. **109**, 035301 (2012).
[22] C. Monroe, W. C. Campbell, L.-M. Duan, Z.-X. Gong, A. V. Gorshkov, P. W. Hess, R. Islam, K. Kim, N. M. Linke, G. Pagano, P. Richerme, C. Senko, and N. Y. Yao, Rev. Mod. Phys. **93**, 025001 (2021).
[23] R. Blatt and C. F. Roos, Nat. Phys. **8**, 277 (2012).
[24] N. Roy, A. Sharma, and R. Mukherjee, Phys. Rev. A **99**, 052342 (2019).
[25] H. Weimer, M. Müller, I. Lesanovsky, P. Zoller, and H. P. Büchler, Nat. Phys. **6**, 382 (2010).
[26] R. Mukherjee, J. Millen, R. Nath, M. P. A. Jones, and T. Pohl, J. Phys. B **44**, 184010 (2011).
[27] R. Löw, H. Weimer, J. Nipper, J. B. Balewski, B. Butscher, H. P. Büchler, and T. Pfau, J. Phys. B **45**, 113001 (2012).

[28] A. Browaeys, D. Barredo, and T. Lahaye, J. Phys. B **49**, 152001 (2016).
[29] M. Morgado and S. Whitlock, AVS Quantum Sci. **3**, 023501 (2021).
[30] J. E. Johnson and S. L. Rolston, Phys. Rev. A **82**, 033412 (2010).
[31] R. Mukherjee, T. C. Killian, and K. R. A. Hazzard, Phys. Rev. A **94**, 053422 (2016).
[32] N. Henkel, F. Cinti, P. Jain, G. Pupillo, and T. Pohl, Phys. Rev. Lett. **108**, 265301 (2012).
[33] R. Mukherjee, Phys. Rev. A **100**, 013403 (2019).
[34] J. B. Balewski, A. T. Krupp, A. Gaj, S. Hofferberth, R. Löw, and T. Pfau, New J. Phys. **16**, 063012 (2014).
[35] J. Zeiher, R. van Bijnen, P. Schauß, S. Hild, J. Choi, T. Pohl, I. Bloch, and C. Gross, Nat. Phys. **12**, 1095 (2016).
[36] H. Bernien, S. Schwartz, A. Keesling, H. Levine, A. Omran, H. Pichler, S. Choi, A. S. Zibrov, M. Endres, M. Greiner, V. Vuletić, and M. D. Lukin, Nature (London) **551**, 579 (2017).
[37] V. Lienhard, S. de Léséleuc, D. Barredo, T. Lahaye, A. Browaeys, M. Schuler, L.-P. Henry, and A. M. Läuchli, Phys. Rev. X **8**, 021070 (2018).
[38] S. Ebadi, T. T. Wang, H. Levine, A. Keesling, G. Semeghini, A. Omran, D. Bluvstein, R. Samajdar, H. Pichler, W. W. Ho, S. Choi, S. Sachdev, M. Greiner, V. Vuletić, and M. D. Lukin, Nature (London) **595**, 227 (2021).
[39] R. Verresen, M. D. Lukin, and A. Vishwanath, Phys. Rev. X **11**, 031005 (2021).
[40] G. Semeghini, H. Levine, A. Keesling, S. Ebadi, T. T. Wang, D. Bluvstein, R. Verresen, H. Pichler, M. Kalinowski, R. Samajdar, A. Omran, S. Sachdev, A. Vishwanath, M. Greiner, V. Vuletić, and M. D. Lukin, Science **374**, 1242 (2021).
[41] P. Scholl, M. Schuler, H. J. Williams, A. A. Eberharter, D. Barredo, K.-N. Schymik, V. Lienhard, L.-P. Henry, T. C. Lang, T. Lahaye, A. M. Läuchli, and A. Browaeys, Nature (London) **595**, 233 (2021).
[42] R. Samajdar, W. W. Ho, H. Pichler, M. D. Lukin, and S. Sachdev, Phys. Rev. Lett. **124**, 103601 (2020).
[43] R. Samajdar, W. W. Ho, H. Pichler, M. D. Lukin, and S. Sachdev, Proc. Natl. Acad. Sci. U.S.A. **118**, e2015785118 (2021).
[44] S. de Léséleuc, V. Lienhard, P. Scholl, D. Barredo, S. Weber, N. Lang, H. P. Büchler, T. Lahaye, and A. Browaeys, Science **365**, 775 (2019).
[45] K. Li, J.-H. Wang, Y.-B. Yang, and Y. Xu, Phys. Rev. Lett. **127**, 263004 (2021).
[46] S. Bettelli, D. Maxwell, T. Fernholz, C. S. Adams, I. Lesanovsky, and C. Ates, Phys. Rev. A **88**, 043436 (2013).
[47] G. Abumwis, M. T. Eiles, and A. Eisfeld, Phys. Rev. Lett. **124**, 193401 (2020).
[48] J. Y. Lee, J. Ramette, M. A. Metlitski, V. Vuletić, W. W. Ho, and S. Choi, Phys. Rev. Lett. **131**, 083601 (2023).
[49] H. Weimer and H. P. Büchler, Phys. Rev. Lett. **105**, 230403 (2010).
[50] E. Sela, M. Punk, and M. Garst, Phys. Rev. B **84**, 085434 (2011).
[51] P. Scholl, H. J. Williams, G. Bornet, F. Wallner, D. Barredo, L. Henriet, A. Signoles, C. Hainaut, T. Franz, S. Geier, A. Tebben, A. Salzinger, G. Zürn, T. Lahaye, M. Weidemüller, and A. Browaeys, PRX Quantum **3**, 020303 (2022).
[52] E. Orignac and R. Citro, Eur. Phys. J. B **33**, 419 (2003).
[53] A. Hayashi, S. Mondal, T. Mishra, and B. P. Das, Phys. Rev. A **106**, 013313 (2022).
[54] D. Rossini and R. Fazio, New J. Phys. **14**, 065012 (2012).
[55] M. Maik, P. Hauke, O. Dutta, M. Lewenstein, and J. Zakrzewski, New J. Phys. **15**, 113041 (2013).
[56] W. P. Su, J. R. Schrieffer, and A. J. Heeger, Phys. Rev. Lett. **42**, 1698 (1979).
[57] B.-L. Chen, S.-P. Kou, Y. Zhang, and S. Chen, Phys. Rev. A **81**, 053608 (2010).
[58] F. Grusdt, M. Höning, and M. Fleischhauer, Phys. Rev. Lett. **110**, 260405 (2013).
[59] K. Sugimoto, S. Ejima, F. Lange, and H. Fehske, Phys. Rev. A **99**, 012122 (2019).
[60] J. Fraxanet, D. González-Cuadra, T. Pfau, M. Lewenstein, T. Langen, and L. Barbiero, Phys. Rev. Lett. **128**, 043402 (2022).
[61] See Supplemental Material at http://link.aps.org/supplemental/10.1103/PhysRevLett.131.203003 for (1) physical parameters for the realization of the setup, (2) mapping of the atomic Hamiltonian to extended Bose-Hubbard model including the dimerized case, (3) additional analysis on verification of individual phases, and (4) numerical method details, which includes Refs. [62–69].
[62] M. Saffman, T. G. Walker, and K. Mølmer, Rev. Mod. Phys. **82**, 2313 (2010).
[63] S. de Léséleuc, Ph.D. thesis, Université Paris-Saclay (ComUE), 2018.
[64] N. Šibalić, J. Pritchard, C. Adams, and K. Weatherill, Comput. Phys. Commun. **220**, 319 (2017).
[65] S. Weber, C. Tresp, H. Menke, A. Urvoy, O. Firstenberg, H. P. Büchler, and S. Hofferberth, J. Phys. B **50**, 133001 (2017).
[66] I. I. Beterov, I. I. Ryabtsev, D. B. Tretyakov, and V. M. Entin, Phys. Rev. A **79**, 052504 (2009).
[67] M. Archimi, C. Simonelli, L. Di Virgilio, A. Greco, M. Ceccanti, E. Arimondo, D. Ciampini, I. I. Ryabtsev, I. I. Beterov, and O. Morsch, Phys. Rev. A **100**, 030501 (2019).
[68] M. Archimi, M. Ceccanti, M. Distefano, L. Di Virgilio, R. Franco, A. Greco, C. Simonelli, E. Arimondo, D. Ciampini, and O. Morsch, Phys. Rev. A **105**, 063104 (2022).
[69] J. Hauschild and F. Pollmann, SciPost Phys. Lect. Notes 5 (2018).
[70] S. R. White, Phys. Rev. Lett. **69**, 2863 (1992).
[71] S. R. White, Phys. Rev. B **48**, 10345 (1993).
[72] X.-J. Yu, S. Yang, J.-B. Xu, and L. Xu, Phys. Rev. B **106**, 165124 (2022).
[73] P. Bak and R. Bruinsma, Phys. Rev. Lett. **49**, 249 (1982).
[74] P. Calabrese and J. Cardy, J. Phys. A **42**, 504005 (2009).
[75] F. Pollmann, S. Mukerjee, A. M. Turner, and J. E. Moore, Phys. Rev. Lett. **102**, 255701 (2009).
[76] F. Köhler, R. Mukherjee, and P. Schmelcher, Phys. Rev. Res. **5**, 023135 (2023).